Investigation of Stator and Rotor Slits' Effects to the Torque and Efficiency of an Induction Motor

Serdal ARSLAN [1], Sibel AKKAYA OY [2], İlhan TARIMER [3]

[1]*Birecik Vocational Higher School, Harran University, Birecik, Turkey*
[2]*Faculty of Marine Sciences, Ordu University, Ordu, Turkey*
[3]*Faculty of Technology, Muğla Sıtkı Koçman University, Muğa, Turkey*

Abstract—**Induction machines have a simple structure and are popular due to their wide range of use, however they have limited power factor and efficiency. Although the working principles of inductions machines have not changed for years, the materials and geometric structures used have undergone significant changes. In this study, slits were applied in the middle of the rotor teeth, rotor-stator teeth and stator teeth of a 7.5 kW induction motor. For these three situations, the torque ripple, iron losses, copper losses, inductance, phase current and voltage inducted in the windings and flux change were analyzed associated with the change in the slit width and slit height. Due to the fact that it is difficult to analytically calculate the slitted models created, they were analyzed by software which uses the finite elements method. The stator-rotor slitted structure determined as the optimum (the one with highest efficiency) and the original motor were compared with 2D and 3D analyses. According to this comparison, a decrease in torque rupture and loss of copper is observed. The motor's torque increased by 27%, and efficiency increased by 4%.**

Keywords: **Stator, rotor, slit, induction motor, efficiency, dimension.**

1. Introduction

Induction motors have an important place both in our modern lives and in the industry due to their simple structures and low costs. A saving in 1% of the amount of energy consumed by the induction motors worldwide would save an energy of 20 billion kWh annually and this amount equals to the amount of energy obtained from 36.5 million barrels of petroleum [1]. The fact that the energy consumed is this high attracts the attention to the three-phase induction motors.

As it is known, although the working principles of induction motors have not changed for years, the materials used and their geometric structures have undergone significant changes. This way, new perspectives arrived in the design of machinery and their fields of application were extended. Also, the International Electrotechnical Commission (IEC) proposed a standard referrence to the energy efficiency classes for electric motors [2]. The use of copper and aluminum in the rotor windings in the induction motors effects the motor performance [3]. Also, using new materials (amorphous materials, etc.) instead of the usual core materials in use increased their efficiency and performance in the medium-high frequency values [4-5]. They are not preferred due to their material cost and difficulty in production. For this reason, the studies on the geometric structure of the induction motors are increasing. Zhou et al. [6] performed the dynamic analysis of the three-phase and one-phase induction motors using the Ansoft Maxwell software and compared the results with the application results. The results that they obtained from the rated speed and locked rotor tests were found to be very close to the simulation results. Aho et al. [7-9] have designed induction motor with rotor structure on the steel slitted solid motor model and found that the slit depth increases the moment of the motor but decreases the mechanical strength. Nerg et al. [10] analyzed the effect of the number of slits in solid-structured rotor

on torque change and unbalanced magnetic pull. They found that a single number of slit in the rotor decreases the ripple that occurs in torque. Zaim [11] found that it is necessary to make an appropriate choice on the slit depth, width and number of the rotor slitted induction motor. In his study, Uzhegov [12] stated that to reduce the rotor impedance and improve the torque and power factor of the machine, a solid rotor with copper end rings could be used. Slitting of the rotor improves flux penetration into the rotor. His work was the development of an easy tool for the high-speed motor with four different types of solid-rotor preliminary designs. Asım [13] proposed an induction motor design with slitted rotor and stator and in this model; he found an improvement in the moment, power factor and efficiency with the increase in the useful flux. In their study using the packaged software, Asım et al. [13-15] found that the optimum slit depth to be performed on the rotor and stator as 15 mm and 0.1 mm since the inducted moment is directly proportional with the rotor resistance whereas inversely proportional to the stator and rotor leakage reactance.

In this study, slits were applied in the middle of the teeth in the rotor, rotor-stator and the stator of 7.5 kW induction motor. These power values are widely used in the industry. In addition, the rotor and stator tooth structure is suitable for slitting the engine selected for this. For these three situations, the torque ripple, iron losses, copper losses, inductance, phase current and voltage inducted in the windings, the flux change were analyzed depending on the change in the slit width and slit height. Due to the fact that it is difficult to analytically calculate the slitted models created, they were analyzed by the ANSYS/MAXWELL software which uses the finite elements method (FEM). Slitted structures selected as the optimum ones were compared with the original motor model. This way, their effects on the efficiency and torque were examined by slitting on the core (stator, rotor or stator-rotor) without changing the stator, rotor slot geometries.

2. Finite Elements Method

In our day, the finite elements method is one of the most preferred method in the solution of the complex electromagnetic field problems. Ansys-Maxwell is the packaged software which can perform electromagnetic analysis, find a solution using the finite elements method and it is widely used. With Maxwell 3D, the actual three dimensional structure of the system is considered. The analysis time of 3D model would be long due to meshing. The 2D analysis was preferred for this reason and for the

reason that studying on the smallest symmetry of the geometry would save time and computer power since it is possible to add thickness data and a symmetry factor. The motors can be divided into smaller parts such as 4/1, 8/1, 16/1 (Figure 2.) and axial symmetries can be used having the pole number under consideration. However, a two dimensional axisymmetric problem definition offers the possibility to analyze the end ring parameters (ring resistance and inductance). Using a three dimensional approach, the correct influence of the bar currents can be taken into account. Furthermore, the three dimensional approach is necessary to calculate the stator end winding inductance and the coupling between end ring and stator end winding [16]. For this reason, 3D analyses were also performed. The analytic solutions were obtained by entering the fundamental dimensioning parameters of induction motor in the modules of the packaged electromagnetic software.

In his paper, Tarımer designed and analyzed 1-phase and 3-phase induction motors [17] by using design toolsets for obtaining motor's magnetic flux distributions, meshing and performance characteristics.

As it is seen in Figure 1., the corresponding machinery type, the fundamental parameters (number of poles, reference speed, and friction-wind loss) are entered and the fundamental dimensioning sizes of the stator and rotor are entered. The motor is prepared for analysis by determining the slot, winding shape and rotor pole shape. However, certain fundamental parameters (mode of working, rated power, operating speed and temperature, rated voltage) should be entered. In order to make the numerical solutions, the appropriate geometry which was analytically determined is brought to the solution by being automatically selected as transient or magnetostatic state by the user. The flowchart of the operation of this software is given in Figure 1.
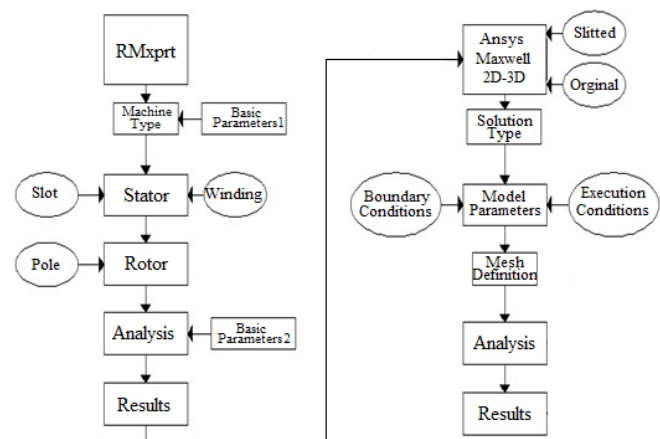

Figure 1. Flowchart of operation of the finite elements method

In Maxwell 2D, first, the size to be designed for the machine's geometry is chosen. The machine geometry is created according to the geometrical data calculated or it is automatically assigned by RMxprt. The models in the symmetrical structure can give all the analysis results on one piece. For the analysis to be fast in this design, the quartic symmetrical model is formed. The model parameters are given as the boundary conditions (for 2D analysis, Az=0 is assigned), number of winding and resistance-inductance parameters (which are automatically assigned by RMxprt). The machine designed is made ready for the analysis. Mesh definition, although seems to have little place in the software algorithm, is very important for the machine to give to an adequate solution. The unknown magnitudes (potential, electric field ...) at each mesh region are represented by scalar or vectorial partial differential equations. According to the analysis algorithm, the finite elements mesh is formed first in the system to be modeled.

In the solution process, the error is reduced and the meshes are improved by iterations. Before starting the field solution, the simulation of the conduction current is performed and the field solution starts. Each element is expressed as a second degree quadratic polynomial. The mesh structure is given in Figure 2.
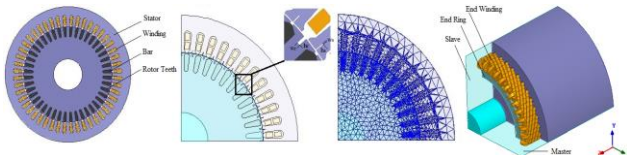

Figure 2. Two and three-dimensional view of the induction motor (halfAxial=1, fractions=4) and the mesh structure generated for the finite element solution

The magnetic field strength (H) in the midpoint of the three edges and in the three corners of each triangular element in the finite element mesh is calculated by using the current density. In the case where the magnetic core material is not linear, the Newton-Raphson method is used to find the magnetic field strength. Also, in order to solve a problem which is not linear with a linear approach, the B-H curve of the material is used. With this approach, proximate solutions are obtained for the nonlinear solution of H. The solver writes the incomplete solution in a file and performs the error analysis. The solver reduces the most erroneous tetrahedral elements with adaptive analysis and continues the solution until the identified error criterion is fulfilled. As a result, the current density, magnetic field strength, magnetic flux density and forces are obtained.

In order to determine the field quantities in the electrical and magnetic manners, the following equation should be solved [6]:

$$\nabla x v \nabla x A = J_s - \sigma \frac{\partial A}{\partial t} + \sigma \nabla V + \nabla x H_c \qquad (1)$$

where; v denotes the speed of the rotating part, A is the magnetic vector potential, J_s is the source current density (one component in z direction for 2D), is the specific magnetic resistance, V is scalar potential on the cross section of a conductor, and H_c is the coercivity of the permanent magnet. This is obtainable at each time step at every node in the finite element model.

In above equation the motion is contained implicitly in the total derivative of A. The transient motion simulator generates rotational motion solutions based on the following motion equation [6];

$$J\beta + \lambda\omega = T_{em} + T_{load} \qquad (2)$$

where; J is the moment of inertia, in kg.m2; T_{em} is the computed electromagnetic torque, in N.m; T_{load} is the external load torque, in N.m.; ω is the angular speed, in rad/s; λ is the angular acceleration, in rad/s2; β is the damping factor, in N.m.s.

External applied torque may either be load torque or may be an accelerating driving torque in the same direction as the electromagnetic torque.

The 2D analyses are performed using computers with I7 CPU, 10GB RAM and recording the steps of 0.0002 sec in the interval 0-0.2 sec, and 3D analyses by recording the steps of 0.0002 sec in the interval 0-0.1 sec. Recording of the steps are important for the analysis to continue from where it left off in case of power cut or program error. However, the software need data area in the hard disk to perform the analysis requested, which depends on the number of mesh and the type of analysis.

Table 1. The Number of 2D and 3D Meshes and Solution Time

Motor Types	2D Meshing	Solution Time [I7 CPU, 10GB RAM]	3D Meshing	Solution Time [I7 CPU, 10GB RAM]
Stator and Rotor Slitted Motor	10532	2hr 58min	178767	80hr 14min
Reference Motor	10123	2hr 10min	143421	62hr 57min

The electromagnetic force of electric machinery is calculated by the stress tensor method of Maxwell. The force is calculated by the two components (radial and tangent) of the magnetic flux density along the line chosen in the two-dimensional finite elements method. These forces are [18-20] given in below equations:

$$F_{\tan} = \frac{L_{stk}}{\mu_0} \oint B_t B_n dl \qquad (3)$$

$$F_{rad} = \frac{L_{stk}}{2\mu_0} \oint_l \left(B_n^2 - B_t^2\right) dl \qquad (4)$$

where; B_t and B_n represents the tangential and normal component of the flux density in the air gap, L_{stk} is the stack length of the motor and l represents the line containing the object.

The rotor slit width (w_r), rotor slit height (h_r), stator slit width (w_s), and the stator slit height (h_s) are chosen as to parametrically vary. The slit width and height applied to the induction motor are w_r, w_s and

h_r, h_s which changed by 1.4 mm and 25 mm, respectively, such that there is no magnetic saturation. As the slit width increases, the magnetic flux density increases in the tooth regions and consequently, the efficiency decreases in these regions since saturation occurs. Thus, the slit width is limited to 1.4 mm [13]. The motor parameters are given in Table 2:

The harmonic activity of a nonlinear receiver can be found as a percentage (%) with "Total Harmonic Distortion (THD)" using the equation 6 [21]:

$$I_H = \sqrt{\left(I_2^2 + I_3^3 + ... + I_n^2\right)} \qquad (5)$$

$$THD = \frac{I_H}{I_T} \qquad (6)$$

where; I_H expresses the current harmonics, and I_T expressed the RMS value of the current in the fundamental frequency component.

Table 2. Motor Parameters

Rated Output Power (*kW*)	7.5	Stator/Rotor Steel Material	M19	Number of Stator Slots	48
Rated Voltage (*V*)	380	Outer Diameter of Stator (mm)	210	Number of Rotor Slots	44
Frequency (*Hz*)	50	Inner Diameter of Stator (mm)	148	Rotor Resistance (ohm)	0.524174
Given Speed (*rpm*)	1452.19 /360	Inner Diameter of Stator (mm)	48	Stator Resistance (ohm)	0.669482
Number of Poles	4	Length of Stator Core (mm)	250	Stator Leakage Reactance (ohm)	0.616379
Winding Connection	Wye	Air Gap (mm)	0.35	Rotor Leakage Reactance (ohm)	0.827093

3. Simulation Results

Unlike the previous studies, in this study, the induction motors with only rotor slitted, only stator slitted and both rotor and stator slitted are examined. The data obtained from the analyses made is used in the temporary time analysis as the data where the motor is in steady state. As seen in Figure 3., in the induction motor with only rotor or only stator slitted, as the slit width and height increases, electro magnetic torque decreases. In each of the analyses, the height and width values vary linearly.
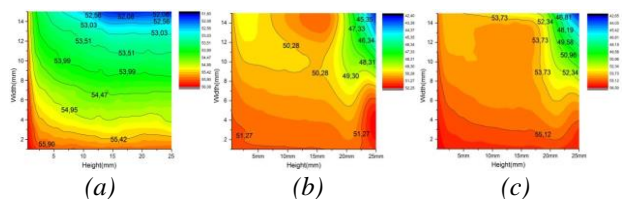

(a)   *(b)*   *(c)*

Figure 3. The values of torque (N.m.) for the structure depending on the slit width and height: (a) Rotor-slitted, (b) Stator-slitted, (c) Rotor-stator slitted.

Figure 4. shows sum of iron and copper losses for the structure depending on the slit width and height. Figure 5. shows maximum initial current for the structure depending on the slit width and height. Figure 6. shows rated current for the structure depending on the slit width and height. Figure 7. shows one phase maximum FluxLinkage value for the structure depending on the slit width and height respectively.
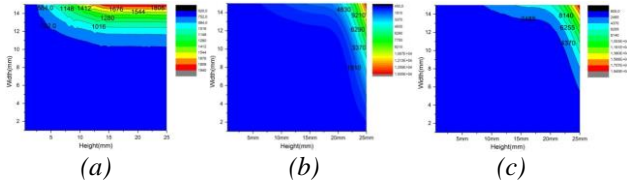

(a)   *(b)*   *(c)*

Figure 4. Sum of iron and copper losses (W) for the structure depending on the slit width and height:(a) Losses for the structure with rotor slitted, (b) Losses for the structure with stator slitted, (c) Losses for the structure with rotor - stator slitted.
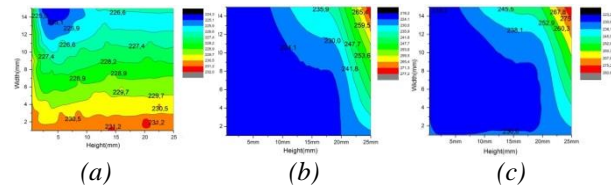

(a)   *(b)*   *(c)*

Figure 5. Maximum initial current (A) for the structure depending on the slit width and height:
(a) Maximum initial current with rotor slitted,
(b) Maximum initial current with stator slitted,

(c) Maximum initial current with rotor and stator slitted.
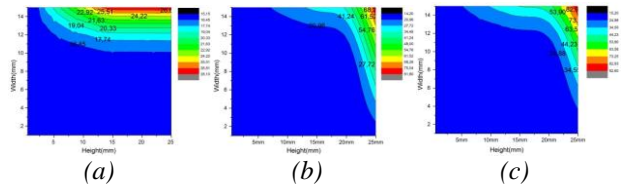

(a)   *(b)*   *(c)*

Figure 6. Rated current (A) for the structure depending on the slit width and height: (a) Rated current with rotor slitted, (b) Rated current with stator slitted, (c) Rated current with rotor and stator slitted.
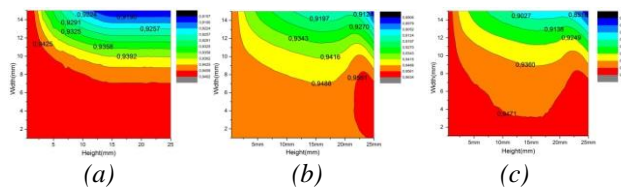

(a)   *(b)*   *(c)*

Figure 7. One phase maximum FluxLinkage (Wb) value depending on the slit width and height: (a) One phase maximum FluxLinkage value with rotor slitted, (b) One phase maximum FluxLinkage value with stator slitted, (c) One phase maximum FluxLinkage value with rotor and stator slitted.

Also, according to the results obtained above, the slit dimensions with the maximum efficiency output by changing the slit dimensions in the stator and rotor geometries are given in Table 3:

Table 3. Comparison table of the slitted motor versus original motor.

	Original Motor (RMxprt)	Original Motor (2D FEM)	Original Motor (3D FEM)	Rotor/Stator Slitted (Hr=2,5mm, Wr=0,9mm / Hs=2.5mm, Ws=0,3mm) (2D FEM)	Rotor/Stator Slitted (Hr=2,5mm, Wr=0,9mm / Hs=2,5mm, Ws=0,3mm) (3D FEM)
Torque (N.m.)	49.317	52.24	38.92	52.29	49.44
Torque Ripples (N.m.)	-	24.82	23.40	17.05	18.51
Iron Losses (W)	153.384	135.34	130.55	133.13	140.5
Rotor and Stator Total Copper Losses (W)	658.70	719.54	846.43	731.03	764.9
Maximum Magnetic Flux Wb)	-	0.9582	0.9613	0.9561	0.9505
Phase Flux (Wb)	14.2959	15.51	12.85	15.48	15.07
Maximum Startup Current (A)	-	231.2	206.94	229.14	207.08
Efficiency (%)	89.4069	89.5	84.89	89.42	88.44
Average Total Weight (kg)	52.7565	52.7565	52.7565	52.475	52.475

Although in his study, Yetgin [13] found the slit dimension that gives the maximum efficiency when the rotor-stator slit width are changed at the same percentage to be 15 mm and 0.1 mm, the rotor and stator slit widths are changed independently in our study. This way, the slit dimension which will give the maximum efficiency in case where the rotor and stator slit dimensions are different is determined. The approximate tooth height of the stator must be selected so as the slit height. When Table 3 is studied, the efficiency obtained from the 2D analyses of the slitted and reference motors are found to be approximately equal to each other. Since the three dimensional model takes into account the end-winding effect and eddy losses that occur in the rotor bars, similar complex structures (slitted, solid, slitted solid, etc.) also need to undergo three-dimensional analysis. In the three-dimensional slitted model, the torque has increased compared to the original motor and even though the torque ripple has decreased, efficiency shows an increase of 4.1%. Total weight has showed little variation since the slit dimensions were small. The magnetic flux density in the slitted and slitless air gap is given in Figure 8. The 5th harmonics not only do they cause losses, but also produce opposite torques in the motor and may overload motor if their amplitude is very big.
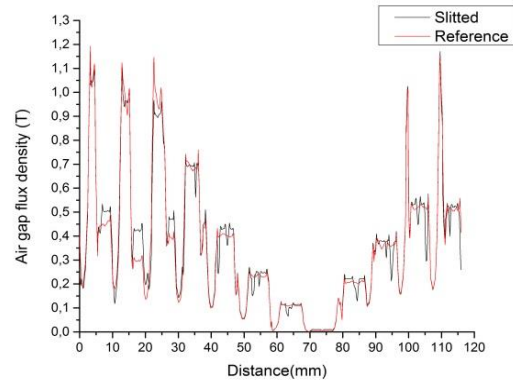

Figure 8. The variation of magnetic flux density in the slitted and slitless air gap with 2D analysis (at 0.2 sec)

The 7th harmonic causes more loss and consequently cause more temperature rise in the motor and its torque is in the same direction of first harmonic torque direction [22]. The harmonic analysis of the current of phase A is performed in between the steady state (0.1sec – 0.2sec) according to the operation cases of full load and no load for the slitted and slitless motors. The Hann function is chosen (Windowing function) because sine wave or combination of sine waves are chosen for general-purpose applications. THD values are calculated using equations 5-6. The magnitude and frequency values obtained are given in Table 4:

Table 4. Harmonic magnitude values of current for slitted-slitless motor (in 2D analysis)

Harmonic Degree	Frequency (Hz)	Reference (No load) THD=%2.65	Slitted (No load) THD=%2.99	Reference (Full load) THD=%2.88	Slitted (Full load) THD=%3.27
1	50	10.754919243306443	10.840194461448633	10.530167912962735	10.644977928898561
3	150	0.001480507267028	0.003797868551232	0.002807185716543	0.003678182774817
5	250	0.284445967180702	0.324047334259645	0.301918272734158	0.346691358893008
7	350	0.005977873663509	0.021598961358879	0.014167132485080	0.020151915186432
9	450	0.002290054683291	0.002618772351868	0.002876059335606	0.001331608817449
11	550	0.005230996448146	0.006183552459047	0.003081521204894	0.005205139720963
13	650	0.004070835722586	0.004869841906463	0.002500960075917	0.001052486465963
15	750	0.002968959178311	0.002189537805050	0.005209086954492	0.002036496365817
17	850	0.006796828035689	0.005638888935200	0.003924481486473	0.001125679580020
19	950	0.007918500048891	0.002861691072247	0.001879246654917	0.003147768604070
23	1150	0.007869255670270	0.001398561375185	0.031425235360150	0.022718829800130
25	1250	0.008853925140022	0.006659716723525	0.007372772018711	0.004566285527429

As can be seen from Table 4., the 5th harmonic is dominant in the phase current in the slitted and slitless structured motor. However, since it is greater than three times of the 7th harmonic effect in the slitted structure, the slitless motor has a smaller THD. Figures 9-10 show variations of the force on the motor in Z and Y directions; Fig. 11. shows variations of the resultant force on the motor respectively.
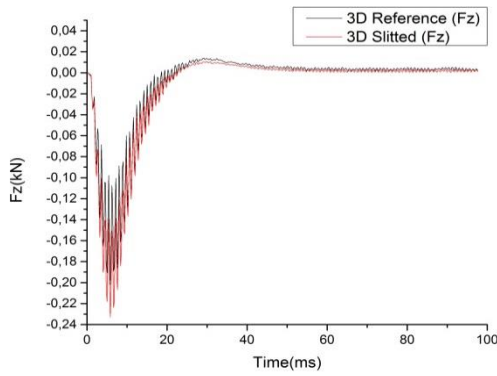
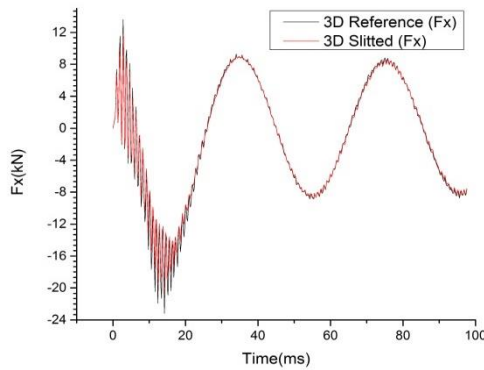*Figure 9. 3D Variation of the force on the motor in Z direction*

Figure 10. 3D Variation of the force on the motor in X direction
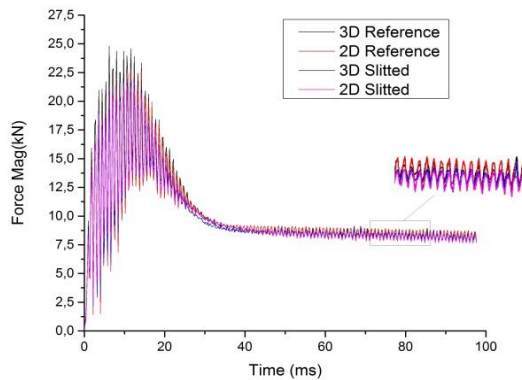

Figure 11. 2D-3D Variation of the resultant force on the motor

Magnetic saturation is major influence on the operating characteristics during transients [23]. Besides, although comparisons in literature with 2D finite elements method and application results have small error [24], it is necessary to conduct 3D temporary time analysis in order to calculate final coil effects for rotor/stator or for different positions of rotor-stator and kernel saturation effects in temporary time analysis. For this reason, 3D transient analyses were performed. Magnetic flux density distributions are given in Figure 12:
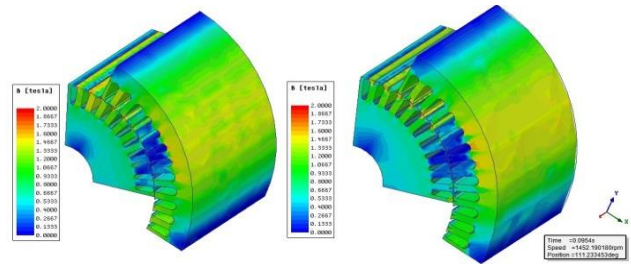

Figure 12. Magnetic flux density distribution in the Reference Motor (left) and Slitted Induction Motor (right)

As can be seen in Fig. 12., the flux density at the statistical curve of the split model showed an increase of about 0.2T. However, the density of the flux in the rotor is about the same as the original motor and the rotor teeth do not reach magnetic saturation. Also, the fact that iron loss is close to the values supports this result.

The advantages of proposed slitted construction according to reference motor are given in Table 5. as comparing original motor. This Table was created considering three-dimensional models.

Table 5. Advantages of the designed motor. Stator-Rotor Slitted Motor.

Motor General Outputs	Difference values
Torque (*N.m.*)	27.02
Torque ripples (*N.m.*)	-20.89
Iron Losses (*W*)	7.62
Rotor and Stator Total Copper Losses (*W*)	-9.9
Maximum Start-up Current (*A*)	0.06
Efficiency (%)	4.1
Approximate Total Weight (*kg*)	-0.5

From Table 5., it has been seen that the performance at the nominal operating points has improved. Because the magnetic flux was effectively used at all the working areas. Beyond this, saturation has been reduced; flux at the teeth has been properly distributed and reaction at the rotor has been reduced. The efficiency of the slitted motor has been improved since the copper losses have been decreased.

4. Conclusion

In this study, the electromagnetic analyses of the induction motor with slitted stator–rotor geometries were performed. It has been seen that it increased the efficiency for it to have rotor slitted or stator-rotor slitted. Since the induction motors have different slot structures, different parametrical analyses need to be made for each induction motor. However, since the noise, temperature and mechanical parameters are effected, these analyses need to be made. For this reason, the force variation for the slitted and slitless structures are also examined in this study.

It is inferred that the force acting on the motor is smaller in the slitted structure than in the reference motor. In the case when they operate at the same speed, torque has increased by 27% while efficiency has increased by 4.1. Moreover, the ripple in torque has decreased by 20.8%. In order for the magnetic saturation does not occur in the core tooth and yoke of the induction motor, to the magnetic flux density values at these regions must be paid attention.

In the study conducted, the graphs are not given, since no magnetic saturation is observed in the tooth and the yoke. It is also obvious that the cost and workmanship of the slitted model would increase. For small power motors, the initial construction cost is slightly high owing to cut off the core with laser. For big power motors, there will be no extra cost due to the new mold to be created for mass production. Besides, although comparisons in literature with 2D finite elements method and application results have small error, it is necessary to conduct 3D temporary time analysis in order to calculate final coil effects for rotor/stator or for different positions of rotor-stator and kernel saturation effects in temporary time analysis.

References

[1] Baykal R. (2011). The Energy Efficiency Application on the Asynchronous Motors. Master's Thesis, University of Marmara University, Turkey.

[2] CEI 60034-30 Standard: Rotating electrical machines - Part 30: Efficiency classes of single-speed, three-phase, cage-induction motors (IE-code). Edition 1.0 2008.

[3] Tudorache, T., & Melcescu, L. (2009). FEM Optimal Design of Energy Efficient Induction Machines. *Advances in Electrical and Computer Engineering, 9(2)*, 58.

[4] Jianwei, L. & Ting, L. (2010). Comparison and Analysis of Classical Motor with Amorphous Iron Motor Based on Ansoft. *Second International Conference on Intelligent Human-Machine Systems and Cybernetics, 1,* 305-308.

[5] Tarımer, İ., Güven, M.E., & Arslan, S. (2012). Investigation for Losses of M19 and Amorphous CoreMaterials Asynchronous Motor by Finite Elements Methods. *Elektronika Ir Elektrotechnika, 18(9),* 15-18.

[6] Zhou, P., Stanton, S., & Zoltan, C. J. (1999). Dynamic Modeling of Three Phase and Single Phase Induction Motors. In: Electric Machines and Drives. *International Conference IEMD'99, Seattle, WA,* 556-558.

[7] Aho, T., Sıhvo, V., Nerg, J., & Pyrhonen, J. (2007). Rotor Materials for Medium-Speed Solid-Rotor Induction Motors. *Electric Machines & Drives Conference, IEMDC '07, 2007, Antalya,* 525-530.

[8] Aho, T., Nerg, J., & Pyrhonen, J. (2005). Influence of Rotor Slit Depth on the Performence of the Solid Rotor induction motor. *Energy Efficiency in Motor Driven Systems Conference Proceedings, 1,* 81-89.

[9] Aho, T., Nerg, J., & Pyrhonen, J. The Effect of the Number of Rotor Slits on the Performance Characteristics of Medium-Speed Solid Rotor Induction Motor. *Power Electronics, Machines, and Drives the 3rd IET International Conference, Ireland,* 515-519.

[10] Nerg, J., Aho, T. & Pyrhönen, J. (2006). Effect of Odd Number of Rotor Slits on the Performance of a High-Speed, High-Power, Solid-Rotor Induction Motor. *6th WSEAS/IASME International Conference on Electric Power Systems, High Voltages and Electric Machines (Power '06), Spain,* 100-105.

[11] Zaim, M. E. (1999). Non-linear Models for the Design of Solid Rotor Induction Machines. *IEEE Transactions on Magnetics, 35(3)*, 1310-1313.

[12] Uzhegov, N. (2012). High-Speed Solid-Rotor Induction Machine - Calculation Program. *Lappeenranta University of Technology, Faculty of Technology*, Master's Thesis.

[13] Yetgin, A.G. & Turan, M. (2014). Efficiency Optimization of Slitted–Core Induction Motor. Journal of Electrical Engineering, 65(1), 60-64.

[14] Yetgin, A.G. (2010). Performance Improvement of Induction Motor with Slitted Core Design. *Sakarya University, PhD thesis, Turkey*.

[15] Yetgin, A.G., Turan, M. & Çanakoğlu, A. İ. (2012). A Novel Slitted Tooth Core Design to Decrease Leakage Flux in Induction Motor. *Journal of the Faculty of Engineering and Arcchitecture of Gazi University, 27(3)*, 607-614.

[16] De Weerdt, R. & Belmans, R. (1995). Squirrel Cage Induction Motor end Effects Using 2D and 3D Finite Elements. *In Electrical Machines and Drives, Seventh International, Durham,* 62-66.

[17] Tarımer, İ., (2005). Computer Aided Design of Induction Motor. *Journal of Polytechnic, 8(1),* 19-24.

[18] Islam, R. & Iqbal, H. (2010). Analytical Model for Predicting Noise and Vibration in Permanent-Magnet Synchronous Motors. *IEEE Transactions on Industry Applications, 46(6),* 2346-2354.

[19] Wilow, V. (2014). Electromagnetical Model of an Induction Motor in COMSOL Multiphysics. *Degree project in Electrical Engineering Master of Science, Sweden.*

[20] Krotsch, J. & Bernhard, P. (2012). Radial Forces in External Rotor Permanent Magnet Synchronous Motors with Non-Overlapping Windings. *IEEE Transactions Industrial Electronics, 59(5),* 2267-2276.

[21] Tezcan, M., Yetgin, A. G., Çanakoğlu, A. İ. & Turan M. (2008). Three Phase Induction Motor Design and FFT Analysis. *Electricity - Electronics and Computer Engineering Symposium, Bursa,* 242-246.

[22] Mirzamani, H. O. & Choobar, A. L. (2004). Study of Harmonics Effects on Performance of Induction Motors. 8th WSEAS International Conference on Circuits, Greece, 487-837.

[23] Conradi, A., Schmülling, C. & Schmülling, S. (2013). Investigation on the Effects of Magnetic Saturation in Induction Machines During Transients. GSTF Journal of Engineering Technology (JET), 2(3).

[24] Tudorache, T. & Melcescu, L. (2009). FEM Optimal Design of Energy Efficient Induction Machines. *Journal: Advances in Electrical and Computer Engineering, 9(2),* 58-64.